

Strengthening Mechanisms of Rail Steel under Compression

Yurii Ivanov ^{1,*}, Mikhail Porfiriev ², Victor Gromov ², Natalia Popova ³ and Yulia Shliarova ²

¹ Plasma Emission Electronics Laboratory, Institute of High Current Electronics SB RAS, 634055 Tomsk, Russia

² Department of Natural Sciences, Siberian State Industrial University, 654007 Novokuznetsk, Russia; mporf372@gmail.com (M.P.); gromov@physics.sibsiu.ru (V.G.); rubannikova96@mail.ru (Y.S.)

³ Department of Physics, Chemistry and Theoretical Mechanics, Tomsk State University of Architecture and Civil Engineering, 634003 Tomsk, Russia; natalya-popova-44@mail.ru

* Correspondence: yufi55@mail.ru; Tel.: +7-(3822)-491713

Abstract: The evolution of the structure–phase states and the dislocation substructure of rail steel under uniaxial compression to the degree of 50% was studied by transmission electron microscopy. The obtained data formed the basis for a quantitative analysis of the mechanisms of rail steel strengthening at degrees of deformation by compressions of 15, 30, and 50%. Contributions to the strengthening caused by the friction of the matrix lattice, dislocation substructure, presence of carbide particles, internal stress fields, solid solution and substructural strengthening, and pearlite component of the steel structure were estimated. Using the adaptivity principle, which assumes the independent action of each of the strengthening mechanisms, the dependence of the rail steel strength on the degree of plastic deformation by compression was estimated. A comparative analysis of the stress–strain curves $\sigma(\epsilon)$ obtained experimentally and calculated theoretically was performed.

Keywords: stress–strain curve; rail steel; structure; dislocation substructure; strengthening mechanisms; additive yield strength; electron microscopy

1. Introduction

The deformation strengthening of steels is one of the ways to change the structural–phase states and properties characterising the fracture resistance [1–7]. Knowledge of the formation patterns of the structural–phase states and properties of pearlite steel during plastic deformation is necessary to control the process of the deformation behaviour. The importance of the information in this field is determined by the depth of fundamental problems in physical materials science, on the one hand, and the practical significance of the problem, on the other hand, since the rails are made of pearlitic steel [8–19].

At present, the general dependencies that characterise strain hardening attract the most interest, as they can be applied for constructing a theory of this phenomenon, on the one hand, and studying the dislocation mechanisms explaining the observed type of curves $\sigma(\epsilon)$, on the other hand. A certain amount of success in the development of ideas regarding the dislocation structures of bainitic and martensitic steels has been achieved in strength physics. However, we should note that the dislocation steel structure and its evolution during deformation are insufficiently studied. This is especially true of the quantitative parameters of the dislocation ensemble. Little attention is paid to fragmentation processes. Internal stress fields have been examined mainly using the X-ray diffraction method, and local stress fields are understudied [20,21].

The transmission diffraction electron microscopy method, due to the fact of its high resolution, makes it possible to conduct an in-depth analysis of the defects in steels and, therefore, is the most effective means of detailed investigation of the dislocation substructure [22,23]. The development of new special types of rails (for high-speed movement, low-temperature reliability, resistance to contact fatigue and wear, etc.) should be based on the knowledge of the mechanisms of the structural and phase changes and fine



Citation: Ivanov, Y.; Porfiriev, M.; Gromov, V.; Popova, N.; Shliarova, Y. Strengthening Mechanisms of Rail Steel under Compression. *Metals* **2024**, *14*, 9. <https://doi.org/10.3390/met14010009>

Academic Editor: Barrie Mintz

Received: 15 February 2023

Revised: 18 March 2023

Accepted: 12 April 2023

Published: 20 December 2023



Copyright: © 2023 by the authors. Licensee MDPI, Basel, Switzerland. This article is an open access article distributed under the terms and conditions of the Creative Commons Attribution (CC BY) license (<https://creativecommons.org/licenses/by/4.0/>).

substructure under deformation. The mechanisms of rail strengthening at different volumes of the passed tonnage were evaluated in [24–26], and the evolution of lamellar pearlite of rail steel under compression deformation was analysed in [27].

The purpose of this work is a comparative analysis of experimental stress–strain curves $\sigma(\varepsilon)$ and the mechanisms of rail steel strengthening, obtained on the basis of a quantitative assessment, under compression deformation.

2. Materials and Methods

Differentially heat-strengthened rails of the DT350 category manufactured by Evraz West Siberian Metallurgical Plant (Novokuznetsk, Russia), produced from evacuated electric steel E76KhF in accordance with the technical requirements TU 0921-276-01124333-2021, were studied. The chemical composition of the rail steel is shown in Table 1. Five rectangular samples with a size of $5 \times 5 \times 10$ mm were cut from the rail head and subjected to deformation. Uniaxial compression deformation was carried out at room temperature on an Instron 3369 (Great Britain, England, London) testing machine at a loading speed of 1.2 mm/min.

Table 1. Chemical composition of the rail steel, % (wt.).

C	Mn	Si	Cr	P	S	Ni	Cu	Ti	Mo	V	Al
0.73	0.75	0.58	0.42	0.012	0.007	0.07	0.13	0.003	0.006	0.04	0.003

The steel structure was studied using transmission electron diffraction microscopy (JEOL JEM 2100F, JEOL Ltd, Akishimam, Tokio Japan). The objects of research for the transmission electron microscopy (foils ranging in thickness from 150 to 200 nm) were made by the electrolytic thinning of plates cut by methods of the electric spark erosion of metal from the central part of the sample in the direction perpendicular to the compression axis. The structural and phase states of the steel subjected to deformation by 15, 30, and 50% were analysed.

Images of the material's fine structure obtained during its examination by an electron microscope were necessary to identify the morphological components of the structure and their volume fractions; determine the size, distribution density, and volume fraction of the cementite particles, as well as their localisation; and define the parameters of the material's fine structure in each morphological component (scalar ρ and excess ρ_{\pm} dislocation density and amplitudes of the curvature–torsion of the crystal lattice χ and internal stresses).

The volume fractions of the morphological components were determined by the planimetric method measuring the total cross-sectional area of the given structural component on a certain area of the foil [28]:

$$\delta = (1/S_t) \sum_{i=1}^n S_{n_i}, \quad (1)$$

where S_t —total area of the image; $\sum_{i=1}^n S_{n_i}$ —total surface area occupied by the corresponding morphological component of the structure. The volume fractions were defined by the continuous sections of the sample with an area of $\sim 100 \mu\text{m}^2$ at a magnification in the microscope column of $\sim 10,000$ times.

The sizes of the cementite particles and the distances between them were determined in each morphological component by micrographs using direct measurement [29].

In steel deformed to $\varepsilon = 50\%$ in the pearlite of the lamellar morphology (non-destroyed pearlite) only the transverse size of the cementite particles was measured, in a ferrite–carbide mixture (destroyed pearlite), only the diameter was measured and for the fragmented perlite, the longitudinal and transverse dimensions were measured:

$$\bar{R} = \frac{1}{N} \cdot \sum_{i=1}^N N_i R_i; \bar{L} = \frac{1}{N} \cdot \sum_{i=1}^N N_i L_i, \quad (2)$$

where N_i —number of particles in a given size class; R_i and L_i —average transverse and longitudinal particle sizes, in this class; n —number of classes; and N —total number of measurements. The number of measurements ranged from 40 to 50.

The average distance between the cementite particles was determined by the secant method using microphotographs [29].

The volume fraction of the particles of the carbide phases in the body of the structural components was determined using the formula [30]:

$$\delta = V_p / tr^2, \quad (3)$$

where V_p —average particle volume; t —foil thickness; and r —distance between particles.

The scalar density of the dislocations in each morphological component of the steel structure was determined by the following methods [22]. Its values were calculated using the formula:

$$\langle \rho \rangle = \frac{M}{t} \left(\frac{n_1}{l_1} + \frac{n_2}{l_2} \right), \quad (4)$$

where n_1 and n_2 —number of intersections of horizontal and vertical lines with length l_1 and l_2 by dislocations; M —magnification of the micrograph; and t —foil thickness (200 nm).

The average scalar dislocation density was determined taking into account the volume fraction of each type of morphological components of the steel structure according to the formula:

$$\langle \rho \rangle = \sum_{i=1}^Z P_{Vi} \rho_i, \quad (5)$$

where P_{Vi} —volume fraction of the material occupied by the i -th type of morphological component of the steel structure; Z —its volume fraction; and ρ_i —scalar density of the dislocations in this morphological component.

The excess dislocation density was calculated by the disorientation gradient [31]:

$$\rho_{\pm} = \frac{1}{b} \frac{\partial \varphi}{\partial \lambda}. \quad (6)$$

Here, b —Burgers vector; $\chi = \partial \varphi / \partial \lambda$ —amplitude of the curvature–torsion of the crystal lattice, where $\partial \varphi$ —inclination angle of the foil in the microscope column, and $\partial \lambda$ —displacement of the extinction contour.

3. Results and Discussion

The transmission electron microscopy of the thin foils established that the steel structure was represented by pearlite grains of plate morphology (Figure 1a), grains of structurally free ferrite (i.e., ferrite grains that do not contain carbide particles in the bulk phases) (Figure 1b) and ferrite grains, in the volume of which cementite particles were observed mainly in the form of short plates (Figure 1d) and globular particles (Figure 1c). As a rule, the volumes of steel with globular particles and particles in the form of short plates were observed separately, which made it possible to estimate their relative content in the material being equal to 1:10.

It can be noted that the relative volume fraction of the grains of the structurally free ferrite was small and varied from 0.01 to 0.05 of the steel structure. The relative volume fraction of the grains of the ferrite–carbide mixture was significantly weightier, the value of which varied in the range from 0.17 to 0.27 of the steel structure. The dislocation substructure was observed in the grain volume mainly in the form of chaotically distributed dislocations.

The plastic deformation of the steel was accompanied by the fragmentation of the ferritic component of the steel, which became stronger as the degree of deformation increased. At $\varepsilon = 50\%$, the fragmented structure of the steel occupied 0.4 of the volume of the examined foil. As the degree of deformation increased, the average sizes of the ferrite plate fragments decreased, from 240 nm ($\varepsilon = 15\%$) to 200 nm ($\varepsilon = 50\%$).

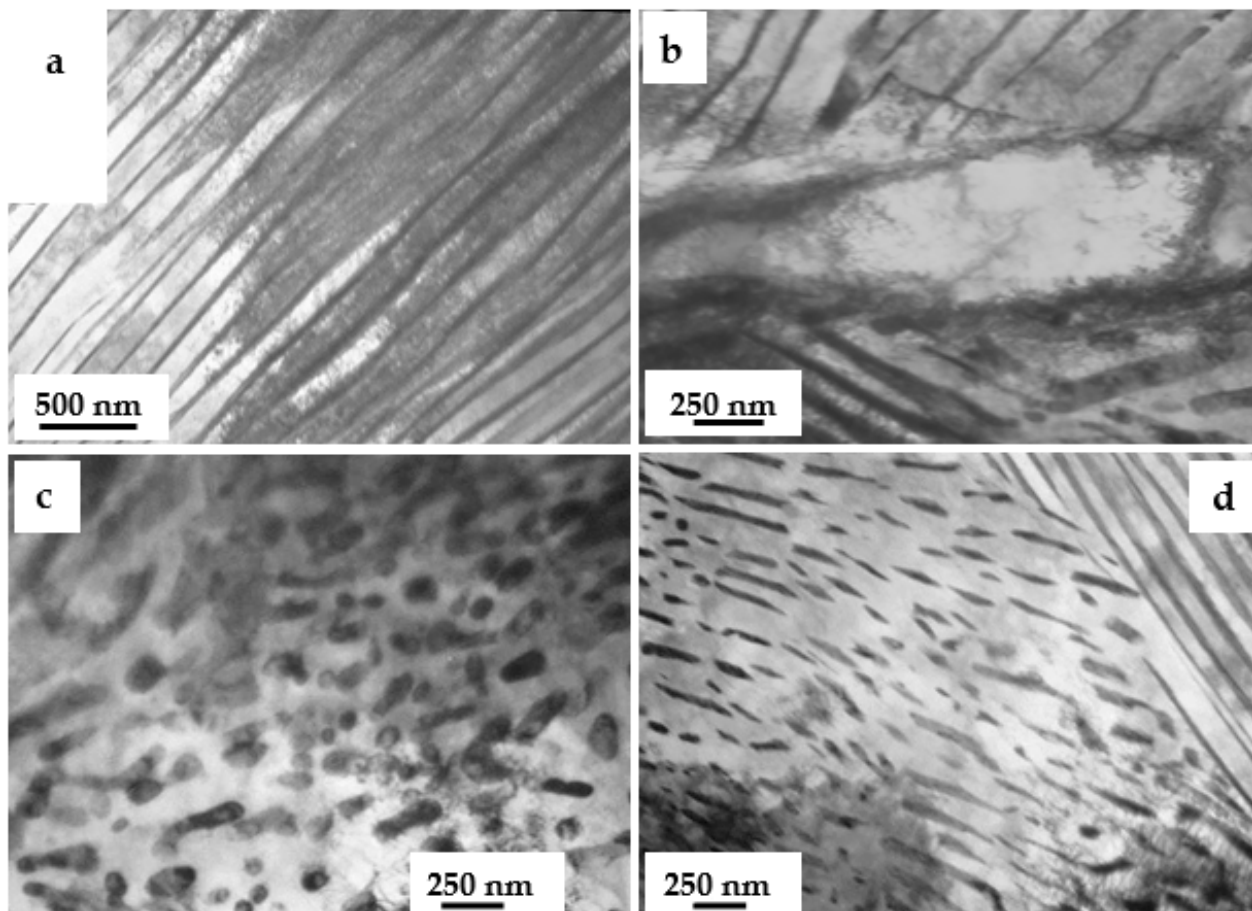


Figure 1. TEM images of the rail structure before deformation ((a)—pearlite grains of plate morphology, (b)—grains of structurally free ferrite, (c,d)—ferrite grains with globular and short plates of cementite).

The analysis of the steel structure by transmission electron microscopy of the thin foils demonstrated the presence of bend extinction contours in the electron microscopic images of the pearlite grains, typical images of which are shown in Figure 2.

The presence of the bend extinction contours indicates the curvature–torsion of the crystal lattice of the analysed foil region. The performed studies show that the sources of the curvature–torsion of the crystal lattice (i.e., stress concentrators) were mainly the interfaces between the ferrite and cementite plates. In most of the observed cases, the contours were located perpendicular to the interface (Figure 2a). The source of the curvature–torsion of the crystal lattice of the material can also be the ends of the cementite plates (Figure 2b,c), as well as the interfaces of the pearlite grains (Figure 2d).

The dissolution and cutting of the cementite plates were observed simultaneously with the fragmentation of the ferrite plates. Carbon atoms, transferred from the cementite crystal lattice to the dislocations, were carried into the interplate space and formed nanoscale (15–20 nm) cementite particles.

In the research literature, two mechanisms of the destruction of cementite plates during the deformation of steel with a pearlite structure are mainly discussed. The first of them consists of cutting the plates by moving the dislocations and carrying carbon atoms into the ferrite in the field of the dislocation stresses (Figure 3a). The estimates show, that in this case, the maximum effect of the cementite decomposition cannot exceed tenths of a percent of the available amount of cementite.

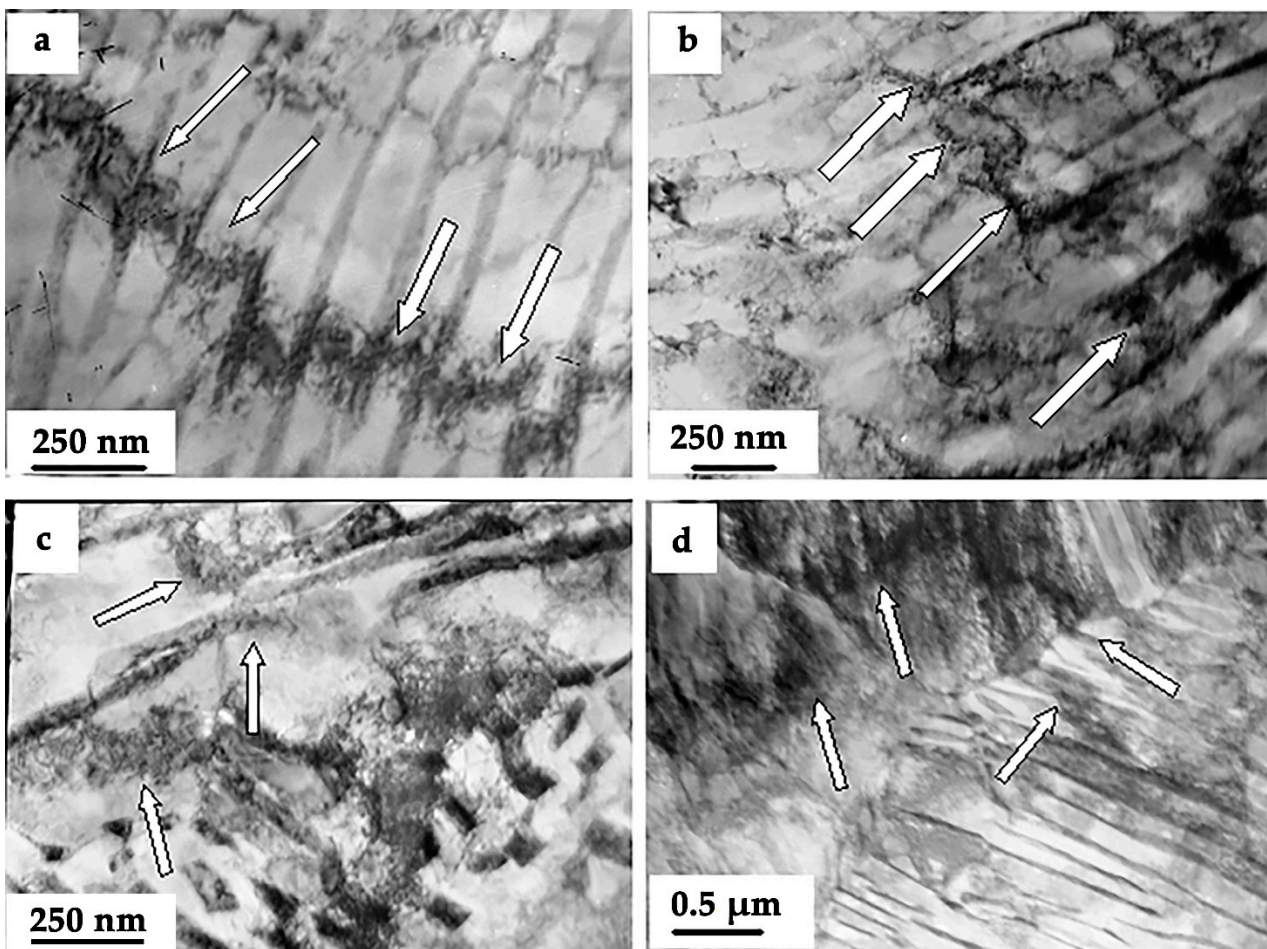


Figure 2. Electron microscopic images of the bend extinction contours (indicated by arrows) ($\epsilon = 30\%$). ((a)—contours are located perpendicular to the interface; source of the curvature–torsion of the crystal lattice: the ends of the cementite plates (b,c), the interfaces of the pearlite grains (d)).

The second mechanism consists of the pulling of carbon atoms from the lattice of the carbide phase during the plastic deformation by dislocations (Figure 3b). Because of a noticeable difference in the average binding energy of the carbon atoms with dislocations (0.6 eV) and with iron atoms in the cementite lattice (0.4 eV), this process leads to the formation of Cottrell atmospheres [27]. In the next stage of the cementite dissolution, the entire volume of the material previously occupied by the cementite plate is filled with nanosized particles. A typical image of the resulting structure is shown in Figure 3c.

The steel deformation was accompanied by the transformation of the dislocation substructure, namely, the quasi-homogeneous distribution of the dislocations of the original steel is replaced by clusters of dislocations around cementite particles.

The samples of the E76KhF steel could not be brought to fracture during the compression test. They were flattened because the steel under study was capable of deforming quite strongly without fracturing. In [27], we showed that the deformation strengthening of the examined steel during the plastic deformation by uniaxial compression has a multistage character.

The revealed transformations of the steel structure will significantly affect the strength and plastic characteristics of the metal, determining the service life of the product. The evaluation of the strengthening mechanisms allows the patterns connecting the parameters of the structure and the strength properties of the material to be identified and the physical nature of the evolution process of the properties to be revealed. The evalua-

tion of the hardening mechanisms was carried out using the widely tested expressions provided below.

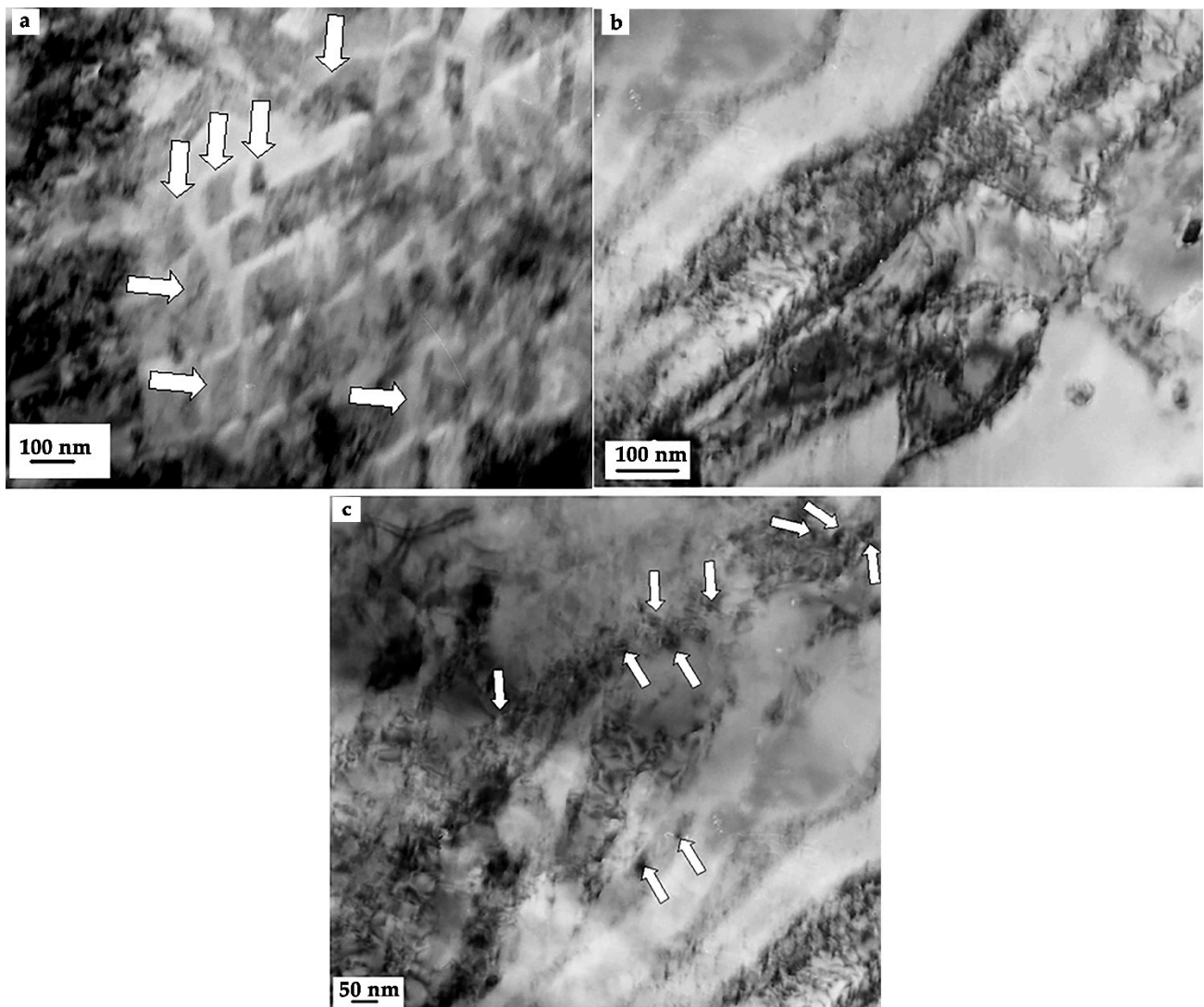


Figure 3. TEM images: (a) structure of a pearlite colony at the stage of the cutting of the cementite plates (indicated by the arrows) by gliding dislocations ($\epsilon = 15\%$); (b) stage of dissolution ($\epsilon = 30\%$); (c) stage of the formation of the nanosized cementite particles (indicated by the arrows) ($\epsilon = 50\%$).

The main contributions to the deformation resistance are as follows [30–33]: $\sigma_0 = 35$ MPa—friction stress of the dislocations in the crystal lattice of α -iron; σ_{ss} —strengthening of a ferrite-based solid solution by atoms of alloying elements; σ_p —strengthening due to the pearlite; σ_h —strengthening by the dislocations “herringbone” that cut the slipping dislocations; σ_{or} —strengthening of the material by incoherent particles when bypassing them with dislocations according to the Orowan mechanism; σ_l —strengthening by the internal long-range stress fields; and σ_s —substructural strengthening.

The evaluation of the solid-solution strengthening of steel caused by carbon atoms and other alloying elements was performed using the empirical expression of the form [30]:

$$\sigma_{ss} = \sum_{i=1}^n C_i k_i, \quad (7)$$

where k_i —strengthening coefficient of the ferrite, which is an increase in the strength of the material at the yield point, with 1 wt.% of the alloying element dissolved in it, the value

of which, for various elements, is determined empirically; C_i —concentration of the i -th element dissolved in ferrite, wt.%. By the i -th element, we mean elements in quantities available at that moment in the α -solid solution.

The hardening caused by the pearlite is determined by the ratio [30]:

$$\sigma_p = k_h(4.75r)^{-1/2}P_V, \quad (8)$$

where P_V —volume fraction of the pearlite; r —distance between the Fe_3C particles; and $k_h = 2 \cdot 10^{-2} \text{ Pa} \cdot \text{m}^{1/2}$ —strengthening coefficient of the ferrite.

The stress required to maintain the plastic deformation, i.e., the stress of the flow σ required to overcome the forces of interaction with stationary dislocations (i.e., dislocations of the “herringbone”) by moving dislocations (i.e., carriers of deformation), is related to the scalar density of the dislocations by the following relation [31]:

$$\sigma_h = m\alpha Gb\sqrt{\rho}, \quad (9)$$

where m —orientation multiplier (or Schmid factor); α —dimensionless coefficient varying within 0.05–0.60 depending on the type of dislocation ensemble (in this work $\alpha = 0.25$, $m\alpha = 1$); G —shear modulus of the matrix material ($G = 80 \text{ GPa}$); b —Burgers vector of the dislocation (0.25 nm); and ρ —the average value of the scalar dislocation density.

Steel strengthening, taking into account the presence of incoherent particles of the second phase, was carried out using the ratio [32]:

$$\sigma_{or} = B \frac{mGb}{2\pi(|r - R|)} \Phi \cdot \ln \left(\left| \frac{r - R}{2b} \right| \right), \quad (10)$$

where R —average particle size; r —distance between particle centres; Φ —multiplier depending on the type of dislocation ($\Phi = 1$); and B —parameter that takes into account the uneven distribution of the particles in the matrix ($B = 0.85$).

Deformation is accompanied by the formation of internal stress fields in the steel. The magnitude of the plastic component of the internal stress fields can be estimated based on the ratio [31]:

$$\sigma_{pl} = m\alpha Gb\sqrt{\rho_{\pm}}, \quad (11)$$

The value of the elastic component of the internal stress fields is estimated based on the ratio [31]:

$$\sigma_{el} = m\alpha Gt\chi_{el}, \quad (12)$$

where t —thickness of the foil, assumed to be 200 nm; χ_{el} —elastic component of the curvature–torsion of the crystal lattice.

It was noted above that the plastic deformation of steel is accompanied by intense material fragmentation. Steel strengthening during the formation of fragments (substructural strengthening) can be estimated based on the ratio [30]:

$$\sigma_s = k_s d^{-1}, \quad (13)$$

where $k_s = 150 \text{ N/m}$; d —size of the formed fragments.

The general steel strengthening in the first approximation, based on the principle of additivity, which assumes the independent action of each of the hardening mechanisms of the material, can be represented as a linear sum of the contributions of the individual strengthening mechanisms [30]. However, in [34,35] it was proved that for dislocation mechanisms acting locally and inhomogeneously inside a single grain, such as σ_h and σ_l , and which turn out to be different in amplitude, place of action, and physical mean-

ing, the summation should be performed in a quadratic approximation. Thus, the total strengthening of the steel should be calculated according to the formula:

$$\sigma = \sigma_0 + \sigma_{ss} + \sigma_p + \sigma_{or} + \sigma_s + \sqrt{(\sigma_l^2 + \sigma_h^2)} \quad (14)$$

The results of the quantitative analysis of the steel structure obtained in this work, as well as in [27], are presented in Tables 2 and 3. This made it possible to evaluate the mechanisms of the steel strengthening both in each morphological component and to determine the role of each contribution to the overall steel strengthening (Table 4).

Table 2. Quantitative parameters of the steel structure in various morphological components with different degrees of plastic deformation.

Structure Parameters	Pearlite			Ferrite	
	Non-Fractured	Fractured	Fragmented	Non-Fragmented	Fragmented
$\varepsilon = 15\%$					
Vol. fraction	70%	24%	3%	1%	2%
Transverse size of the α -phase interlayer, nm	160	120	120		
Fragment size, nm	–	–	120 \times 400	–	400
Fe ₃ C	size, nm	d = 16	12 \times 280	12 \times 160	
	vol. fraction	12%	8.7%	1.5%	
Fraction of carbon	0.8%	0.6%	0.11%		
$\rho_\alpha \times 10^{-10}, \text{cm}^{-2}$	1.91	2.06	2.08	2.21	~0
$\rho_\pm \times 10^{-10}, \text{cm}^{-2}$	1.54	1.96	2.08	2.21	
$\chi = \chi_{pl} + \chi_{el}, \text{cm}^{-1}$	385	490	650 = 520 _{pl} + 30 _{el}	1090 = 550 _{pl} + 140 _{el}	745 = 0 _{pl} + 745 _{el}
$\varepsilon = 30\%$					
Vol. fraction	65%	20%	12%	0	3%
Transverse size of the α -phase interlayer, nm	160	120	120		
Fragment size, nm	–	–	120 \times 200	–	200
Fe ₃ C	size, nm	d = 18	16 \times 280	12 \times 160	
	vol. fraction	12%	4.8%	0.92%	
Fraction of carbon	0.8%	0.34%	0.07%		
$\rho_\alpha \times 10^{-10}, \text{cm}^{-2}$	2.18	2.50	1.59		~0
$\rho_\pm \times 10^{-10}, \text{cm}^{-2}$	1.76	2.26	1.59		
$\chi = \chi_{pl} + \chi_{el}, \text{cm}^{-1}$	440	565	435 = 395 _{pl} + 40 _{el}		745 = 0 _{pl} + 745 _{el}
$\varepsilon = 50\%$					
Vol. fraction	0	60%	40%	0	0
Fragment size, nm			200		
Fe ₃ C in the α -phase (inside fr.)	size, nm	d = 12; r = 16	d = 16; r = 20		
	vol. fraction	1.8%	2.7%		
Fraction of carbon in α -phase		0.12%	0.19%		
Fe ₃ C in the layers of (on border of fr.)	size, nm	d = 14; r = 20	d = 16; r = 30		
	vol. fraction	2.7%	1.2%		
Fraction of carbon		0.19%	0.09%		
$\rho_\alpha \times 10^{-10}, \text{cm}^{-2}$		2.25	0		
$\rho_\pm \times 10^{-10}, \text{cm}^{-2}$		2.25			
$\chi = \chi_{pl} + \chi_{el}, \text{cm}^{-1}$		575 = 560 _{pl} + 15 _{el}	55 = 0 _{pl} + 55 _{el}		

Table 3. Average material parameters of the steel's fine structure at different degrees of plastic deformation.

Average Structure Parameters	$\varepsilon = 15\%$	$\varepsilon = 30\%$	$\varepsilon = 50\%$
$\rho_\alpha \times 10^{-10}, \text{cm}^{-2}$	1.92	2.11	1.35
$\rho_\pm \times 10^{-10}, \text{cm}^{-2}$	1.63	1.79	1.35
$\chi = \chi_{pl} + \chi_{el}, \text{cm}^{-1}$	425 = 410 _{pl} + 15 _{el}	470 = 445 _{pl} + 25 _{el}	365 = 335 _{pl} + 30 _{el}

Table 4. Values of the contributions of the various mechanisms to steel strengthening in various morphological components and in general for the material at different degrees of plastic deformation.

Contributions	Pearlite			Ferrite		In the Material
	Non-Fractured	Fractured	Fragmented	Non-Fragment	Fragmented	
$\epsilon = 15\%$						
Vol. fraction	70%	24%	3%	1%	2%	100%
σ_h , MPa	275	285	290	295	0	273
σ_{pl} , MPa	250	280	290	295	0	254
σ_{el} , MPa	0	0	40	190	1010	20
σ_s , MPa	–	–	550	–	350	25
σ_0 , MPa	35	35	35	35	35	35
σ_{ss} , MPa	80	80	260	1400	1400	130
σ_p , MPa	570	250	0			460
σ_{or} , MPa			135	0	0	5
$\epsilon = 30\%$						
Vol. fraction	65%	20%	12%	0	3%	100%
σ_h , MPa	295	315	250		0	285
σ_{pl} , MPa	265	300	250		0	262
σ_{el} , MPa	0	0	55		1010	35
σ_s , MPa	–	–	835		750	125
σ_0 , MPa	35	35	35		35	35
σ_{ss} , MPa	80	315	190		1400	180
σ_p , MPa	570	250	0			420
σ_{or} , MPa			135			15
$\epsilon = 50\%$						
Vol. fraction	0	60%	40%	0	0	100%
σ_h , MPa		300	0			180
σ_{pl} , MPa		300	0			180
σ_{el} , MPa		20	75			95
σ_s , MPa		–	750			300
σ_0 , MPa		35	35			35
σ_{ss} , MPa		315	300			310
σ_p , MPa		250	0			150
σ_{or} , MPa		1120	645			930

Analysing the results provided in Table 4, we can note, firstly, that the strength of the steel is a multifactorial value and is determined by the combined action of a number of physical mechanisms. Secondly, the strength of the metal rails depends on the degree of deformation by compression. Thirdly, the strength of the metal increases significantly at large degrees of deformation. The results of summing the contributions of the identified mechanisms to the steel strengthening, performed in the additive approximation, are presented in Figure 4b. It is clearly seen that the performed estimates are in good qualitative agreement with the behaviour of the experimental stress–strain curve (Figure 4a). The quantitative discrepancy between the corresponding experimentally obtained and estimated values of steel strength varied within 13–28%. It can be assumed that one of the reasons for this discrepancy is the heterogeneity of the steel structure (the presence of grains of lamellar pearlite and grains of ferrite–carbide mixture), which, having different strengths, will make adjustments to the deformation behaviour of the steel.

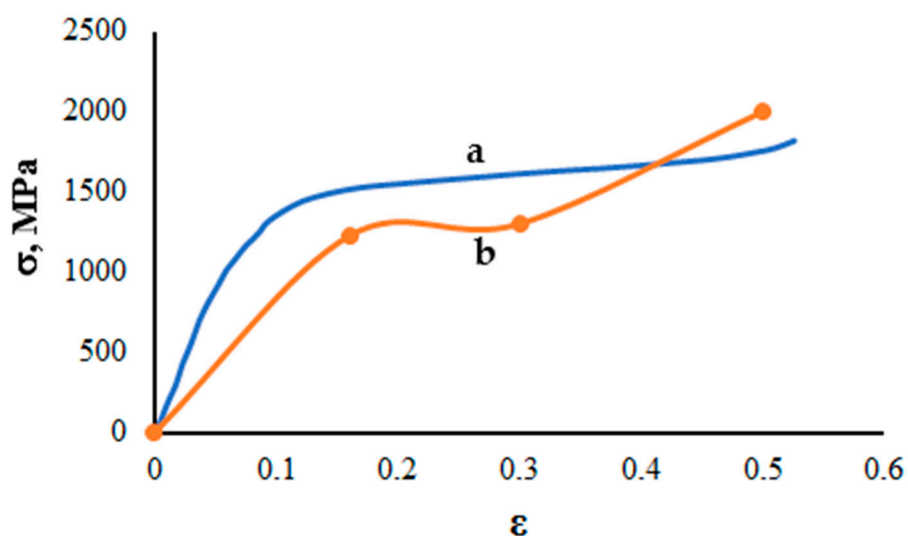


Figure 4. Dependence σ - ϵ of rail steel subjected to uniaxial compression loading: (a) experimental curve; (b) theoretical curve.

4. Conclusions

An evaluation of the strengthening mechanisms at various stages of steel deformation was carried out using the quantitative results of the study of a steel structure subjected to uniaxial compression deformation. It is shown that the main strengthening factor of the examined steel at the initial stage ($\approx 15\%$) is the presence of lamellar pearlite grains. As the deformation degree increases, the role of this factor decreases due to the destruction of the cementite plates. An increase in the deformation degree is accompanied by a decrease in the contribution to the steel strengthening from scalar and excessive dislocation density, which is associated with the drifting of dislocations into the boundaries of fragments. The role of the contribution of the formation of a solid solution (due to the dissolution of cementite), fragmentation (due to the decrease in the size of fragments and an increase in the relative content of the fragmented structure) and incoherent particles of the carbide phase to the steel strengthening rises with the increase in the degree of steel deformation. A good qualitative agreement of the experimentally obtained and calculated values of steel strength was revealed. The revealed quantitative discrepancy between the corresponding experimentally obtained and estimated values of steel strength might be conditioned by the heterogeneity of the steel structure, namely, the presence of grains of lamellar pearlite and grains of ferrite-carbide mixture, which, having different strengths, will make adjustments to the deformation behaviour of the material.

Author Contributions: Conceptualisation, Y.I., V.G. and N.P.; methodology, Y.I.; software, Y.I. and V.G.; validation, M.P. and Y.S.; formal analysis, Y.I., V.G., M.P., N.P. and Y.S.; investigation, Y.I., V.G., N.P., M.P. and Y.S.; resources, Y.I. and V.G.; writing—original draft preparation, M.P. and Y.S.; writing—review and editing, Y.I., V.G. and N.P.; supervision, Y.I. and V.G.; project administration, Y.I. and V.G. All authors have read and agreed to the published version of the manuscript.

Funding: The work was carried out within the framework of the state assignment of the Ministry of Science and Higher Education of the Russian Federation (topic No. FEMN-2023-0003).

Data Availability Statement: Data available on request due to restrictions e.g., privacy or ethical. The data presented in this study are available on request from the corresponding author. The data are not publicly available due to privacy or ethical.

Conflicts of Interest: The authors declare no conflict of interest.

References

1. Bataev, A.; Bataev, I.; Nikulina, A.; Popelyukh, A.; Balagansky, I.; Plotnikova, N. Structural transformations of carbon ferritic-pearlitic steels under conditions of high-speed loading. *Obrab. Metallov—Metal Work. Mater. Sci.* **2019**, *21*, 115–128. [[CrossRef](#)]
2. Klevtsov, G.V.; Valiev, R.Z.; Klevtsova, N.A.; Zaripov, N.G.; Karavaeva, M.V. Strength and fracture mechanisms of nanostructured metallic materials under single kinds of loading. *MiTOM* **2017**, *9*, 54–62. [[CrossRef](#)]
3. Yang, C.; Song, N.; Xiaozhou, L.; Min, S.; Yuntian, Z. Structural evolutions of metallic materials processed by severe plastic deformation. *Mater. Sci. Eng. R Rep.* **2018**, *133*, 1–59. [[CrossRef](#)]
4. Gubicza, J. Lattice defects and their influence on the mechanical properties of bulk materials processed by severe plastic deformation. *Mater. Trans.* **2019**, *60*, 1230–1242. [[CrossRef](#)]
5. Mazilkin, A.; Straumal, B.; Kilmametov, A.; Straumal, P.; Baretzky, B. Phase transformations induced by severe plastic deformation. *Mater. Trans.* **2019**, *60*, 1489–1499. [[CrossRef](#)]
6. Blank, V.D.; Popov, M.Y.; Kulnitskiy, B.A. The Effect of severe plastic deformations on phase transitions and structure of solids. *Mater. Trans.* **2019**, *60*, 1500–1505. [[CrossRef](#)]
7. Bubnov, V.A.; Korotovskikh, V.K.; Kostenko, S.G. Effect of the degree of plastic deformation on hardness of austenitic steel. *Chem. Pet. Eng.* **2022**, *57*, 1038–1042. [[CrossRef](#)]
8. Wang, Y.; Tomota, Y.; Harjo, S.; Gong, W.; Ohmura, T. In-situ neutron diffraction during tension-compression cyclic deformation of a pearlite steel. *Mater. Sci. Eng. A* **2016**, *676*, 522–530. [[CrossRef](#)]
9. Pan, R.; Ren, R.; Chen, C.; Zhao, X. Formation of nanocrystalline structure in pearlitic steels by dry sliding wear. *Mater. Charact.* **2017**, *132*, 397–404. [[CrossRef](#)]
10. Steenbergen, M. Rolling contact fatigue: Spalling versus transverse fracture of rails. *Wear* **2017**, *380–381*, 96–105. [[CrossRef](#)]
11. Vinogradov, A.; Estrin, Y. Analytical and numerical approaches to modelling severe plastic deformation. *Prog. Mater. Sci.* **2018**, *95*, 172–242. [[CrossRef](#)]
12. Nikas, D.; Zhang, X.; Ahlström, J. Evaluation of local strength via microstructural quantification in a pearlitic rail steel deformed by simultaneous compression and torsion. *Mater. Sci. Eng. A* **2018**, *737*, 341–347. [[CrossRef](#)]
13. Skrypyuk, R.; Ekh, M.; Nielsen, J.C.O.; Pålsson, B.A. Prediction of plastic deformation and wear in railway crossings—Comparing the performance of two rail steel grades. *Wear* **2019**, *428–429*, 302–314. [[CrossRef](#)]
14. Rong, K.; Xiao, Y.; Shen, M.; Zhao, H.; Wang, W.; Xiong, G. Influence of ambient humidity on the adhesion and damage behavior of wheel–rail interface under hot weather condition. *Wear* **2021**, *486–487*, 204091. [[CrossRef](#)]
15. Li, X.C.; Ding, H.H.; Wang, W.J.; Guo, J.; Liu, Q.Y.; Zhou, Z.R. Investigation on the relationship between microstructure and wear characteristic of rail materials. *Tribol. Int.* **2021**, *163*, 107152. [[CrossRef](#)]
16. Miranda, R.S.; Rezende, A.B.; Fonseca, S.T.; Sinatora, A.; Mei, P.R. Fatigue and wear behavior of pearlitic and bainitic microstructures with the same chemical composition and hardness using twin-disc tests. *Wear* **2022**, *494–495*, 204253. [[CrossRef](#)]
17. Pereira, H.B.; Dias Alves, L.H.; Rezende, A.B.; Mei, P.R.; Goldenstein, H. Influence of the microstructure on the rolling contact fatigue of rail steel: Spheroidized pearlite and fully pearlitic microstructure analysis. *Wear* **2022**, *498–499*, 204299. [[CrossRef](#)]
18. Pan, R.; Yu, C.; Lan, H.; Shiju, E.; Ren, R. Investigation into the microstructure evolution and damage on rail at curved tracks. *Wear* **2022**, *504–505*, 204420. [[CrossRef](#)]
19. Zhang, S.; Spiriyagin, M.; Lin, Q.; Ding, H.; Wu, Q.; Guo, J.; Liu, Q.; Wang, W. Study on wear and rolling contact fatigue behaviours of defective rail under different slip ratio and contact stress conditions. *Tribol. Int.* **2022**, *169*, 107491. [[CrossRef](#)]
20. Yildirim, C.; Jessop, C.; Ahlström, J.; Detlefs, C.; Zhang, Y. 3D mapping of orientation variation and local residual stress within individual grains of pearlitic steel using synchrotron dark field X-ray microscopy. *Scr. Mater.* **2021**, *197*, 113783. [[CrossRef](#)]
21. Rybin, V.V. Large plastic deformations and destruction of metals. *Metallurgy* **1986**, *12*, 224.
22. Hirsch, P.; Hovey, A.; Nicholson, P.; Pasley, D.; Whelan, M. *Electron Microscopy of Thin Crystals*; Mir: Moscow, Russia, 1968; p. 574.
23. Carter, C.B.; Williams, D.B. *Transmission Electron Microscopy*; Springer International Publishing: Berlin, Germany, 2016; p. 518.
24. Ivanov, Y.A.; Gromov, V.E.; Yuriev, A.A.; Kormyshev, V.E.; Rubannikova, Y.A.; Semin, A.P. Deformation strengthening mechanisms of rails in extremely long-term operation. *J. Mater. Res. Technol.* **2021**, *11*, 710–718. [[CrossRef](#)]
25. Yuriev, A.A.; Ivanov, Y.F.; Gromov, V.E.; Rubannikova, Y.A.; Starostenkov, M.D.; Tabakov, P.Y. *Structure and Properties of Lengthy Rails after Extreme Long-Term Operation*; Materials Research Forum LLC: Millersville, PA, USA, 2021; p. 190.
26. Ivanov, Y.F.; Glezer, A.M.; Kuznetsov, R.V.; Gromov, V.E.; Shliarova, Y.A.; Semin, A.P.; Sundeev, R.V. Fine structure formation in rails under ultra long-term operation. *Mater. Lett.* **2022**, *309*, 131378. [[CrossRef](#)]
27. Ivanov, Y.F.; Gromov, V.E.; Aksenova, K.V.; Kuznetsov, R.V.; Kormyshev, V.E.; Vashchuk, E.S. Evolution of the structure of rail steel under compression. *Deform. Destr. Mater.* **2022**, *8*, 9–14. [[CrossRef](#)]
28. Saltykov, S.A. *Stereometric Metallography*; Defense Technical Information Center: Fort Belvoir, VA, USA, 1976; Volume 3, p. 376.
29. Chernyavsky, V.S. *Stereology in Metal Science*; Metallurgy: Moscow, Russia, 1977; 280p.
30. Goldstein, M.I.; Farber, B.M. *Dispersion Hardening of Steels*; Metallurgy: Moscow, Russia, 1979; p. 208.
31. Koneva, N.A.; Kiseleva, S.F.; Popova, N.A. *Evolution of Structure and Internal Stress Fields. Austenitic Steel*; Lap Lambert Academic Publishing: Saarbrücken, Germany, 2017; p. 148.
32. Yao, M.J.; Welsch, E.; Ponge, D.; Haghghat, S.M.H.; Sandlöbes, S.; Choi, P.; Herbig, M.; Bleskov, I.; Hickel, T.; Lipinska-Chwalek, M.; et al. Strengthening and strain hardening mechanisms in a precipitation-hardened high-Mn lightweight steel. *Acta Mater.* **2017**, *140*, 258–273. [[CrossRef](#)]

33. Tushinsky, L.I.; Bataev, A.A.; Tikhomirova, L.B. *Pearlite Structure and Structural Strength of Steel*; VO "Science"; Siberian Publishing Company: Novosibirsk, Russia, 1993; 280p.
34. Popov, V.E.; Koneva, N.A.; Tereshko, I.V. *Deformation Hardening of Ordered Alloys*; Metallurgy: Moscow, Russia, 1979; p. 256.
35. Kozlov, E.V.; Koneva, N.A. The nature of hardening of metal materials. *Izv. Vuzov Phys.* **2002**, *45*, 52–71.

Disclaimer/Publisher's Note: The statements, opinions and data contained in all publications are solely those of the individual author(s) and contributor(s) and not of MDPI and/or the editor(s). MDPI and/or the editor(s) disclaim responsibility for any injury to people or property resulting from any ideas, methods, instructions or products referred to in the content.